Research paper

Biodegradation of inorganic drug delivery systems in subcutaneous conditions

M. Kovalainen, R. Kamakura, J. Riikonen, M. Finnilä, T. Nissinen, J. Rantanen, M. Niemelä, P. Perämäki, M. Mäkinen, K.H. Herzig, V.P. Lehto

PII: S0939-6411(17)30924-4
DOI: https://doi.org/10.1016/j.ejpb.2017.10.014
Reference: EJPB 12619

To appear in: *European Journal of Pharmaceutics and Biopharmaceutics*

Received Date: 11 August 2017
Revised Date: 16 October 2017
Accepted Date: 18 October 2017

Please cite this article as: M. Kovalainen, R. Kamakura, J. Riikonen, M. Finnilä, T. Nissinen, J. Rantanen, M. Niemelä, P. Perämäki, M. Mäkinen, K.H. Herzig, V.P. Lehto, Biodegradation of inorganic drug delivery systems in subcutaneous conditions, *European Journal of Pharmaceutics and Biopharmaceutics* (2017), doi: https://doi.org/10.1016/j.ejpb.2017.10.014

TITLE: Biodegradation of inorganic drug delivery systems in subcutaneous conditions

AUTHORS:

Kovalainen M[a*], Kamakura R[a], Riikonen J[b], Finnilä M[c], Nissinen T[b], Rantanen J[b], Niemelä M[d], Perämäki P[d], Mäkinen M[e], Herzig KH[a,f,g], Lehto VP[b]

AFFILIATIONS:

[a] Research Unit of Biomedicine & Biocenter of Oulu, Faculty of Medicine, P.O. Box 5000, FI-90014 University of Oulu, Finland

[b] Department of Applied Physics, Faculty of Science and Forestry, University of Eastern Finland, P.O. Box 1627, 70210 Kuopio, Finland

[c] Research Unit of Medical Imaging, Physics and Technology, Faculty of Medicine, P.O. Box 5000, FI-90014 University of Oulu, Finland

[d] Research Unit of Sustainable Chemistry, Faculty of Technology, P.O.Box 3000, FI-90014 University of Oulu, Finland

[e] Cancer Research and Translational Medicine Research Unit, Faculty of Medicine, P.O. Box 5000, FI-90014 University of Oulu, Finland

[f] Department of Gastroenterology and Metabolism, Poznan University of Medical Sciences, Poznan, Poland.

[g] Medical Research Center (MRC) and Oulu University Hospital, Oulu, Finland

*Corresponding author: miia.kovalainen@oulu.fi, fax +358 8 344 084

KEYWORDS: Porous silicon; biodegradation; subcutaneous injection; inorganic drug carriers; controlled peptide delivery; mesoporous materials

ABSTRACT

Despite extensive efforts to develop delivery systems for oral administration, subcutaneous (s.c.) injection remains the most common way to administer peptide drugs. To limit the number of frequent injections, sustained release systems that are easy to produce, suitable for various drugs, safe and biodegradable are urgently needed. Porous silicon (PSi) has been recognized to be one of the most promising materials for s.c. peptide delivery, but its biodegradation in s.c. tissue has not been studied *in vivo,* despite extensive *in vitro* research.

In the present study, differently modified PSi microparticles were injected s.c. in mice, after which the morphology of the particles was thoroughly studied with transmission electron microscopy, micro-computed tomography and X-ray diffraction. Furthermore, histopathology of the s.c. tissue was analyzed to evaluate biocompatibility. To the best of our knowledge, this is the first systematic study which reveals the degradation behavior of various PSi materials *in vivo*.

The PSi surface chemistry significantly affected the biodegradation rate of the s.c. injected microparticles. The most hydrophobic PSi microparticles with hydrocarbonized surface showed the lowest biodegradation rate while the hydrophilic microparticles, with oxide surface, degraded the fastest. The results from different empirical methods complemented each other to deduce the biodegradation mechanism of the inorganic delivery system, providing useful information for future development of s.c. carriers.

1. INTRODUCTION

The number of peptide therapeutics on the market has been steadily increasing and roughly 140 peptides are under clinical trials [1]. However, there are various obstacles that limit the clinical use of peptides, including their poor permeation through biological membranes and short half-life after administration, which can be as short as few minutes. Therefore, despite

the significant advantages peptides offer over low molecular weight drugs, they usually require frequent invasive administration. Subcutaneous (s.c.) injection is the most often used, cost-efficient and rather feasible way to administer peptide drugs, such as insulin. S.c. injection is precise and suitable to be applied by the patient, without need for assistance by a healthcare professional. However, the frequency of injections should be as low as possible, to avoid injection related tissue damage, experienced discomfort and drug related adverse effects to increase patient compliance. Therefore, to improve therapeutic outcomes and patient safety, novel delivery systems for s.c. peptide administration are urgently needed.

It is very important that the drug carrier system does not remain permanently at the injection site. To avoid accumulation of the drug carrier material in the administration site, the carrier should have a sufficient biodegradation rate. When it comes to using s.c. delivery as a mode of administration, the route has its own specialties that should be considered while developing carrier systems for s.c. drug delivery. S.c. space consists of loose connective and adipose tissue, with blood and lymphatic capillaries, and has its own unique characteristics as a delivery route. The circulating solution consists of rather low volumes of interstitial fluid, which exchanges dissolved substances with blood and intracellular fluid, but lacks some of the compartments from plasma. Also, the temperature of s.c. tissue is lower than core body temperature and 34˚C is considered to represent the average temperature in s.c. tissue [2]. These factors create a challenge to investigate the s.c. delivery systems *in vitro* or *in vivo* in an environment that would correspond to the final administration site.

Porous silicon (PSi) is a fascinating nanostructured platform offering numerous possibilities. PSi is under development for a number of biomedical applications ranging from biosensing and imaging applications to chemotherapy, targeted and self-reporting delivery, theranostics and delivery of poorly soluble drugs [3-8]. Nanostructured PSi has been shown to be a promising carrier material for controlled s.c. delivery of Melanotan II prolonging its

pharmacological effects [12]. Furthermore, the release of peptide YY3-36 was sustained over several days, which was also confirmed *in vivo* by demonstrating improved pharmacokinetics [9]. In addition, the particle size, porosity and surface chemistry can be fine-tuned to achieve optimal carrier properties, for example, to control the peptide release [11]. In general, peptides are small biomolecules with dimensions of only few nanometres and insulin (51 amino acids) is often considered as the largest peptide. The pore size of PSi is usually 10-15 nm, which is large enough for peptides and many proteins. The pore size can be modified during fabrication to obtain suitable pore size to control the drug loading and release, as needed. Hence, PSi could be utilized as a carrier system for peptides or other biomolecules with various sizes. In general, the loaded peptide is released by diffusion from PSi when the peptide is in contact with the surrounding solvent, but also the PSi dissolution is expected to play a role in drug release, especially when the PSi surface is hydrophobic or has strong attractive interactions between the loaded peptide and surface [12-14]. It must be noted that *in vivo* and *in vitro* degradation rates of PSi may be different as has been observed also with other biomaterials. For example, *in vitro* degradation of different types of rosin-based films was slower compared with the rate *in vivo* [15, 16]. The faster *in vivo* degradation of the delivery system may even result in unwanted and premature drug release, if the drug release is controlled by the degradation of the carrier material. This is supported by observations showing that complete peptide release from PSi particles has been demonstrated *in vivo* despite the incomplete *in vitro* release [10, 17]. Hence, it is important to investigate the biodegradation of the carrier material at the actual delivery site *in vivo*, since it may have a significant effect on the drug release as well as biocompatibility.

To be used regularly, e.g. weekly or fortnightly, the parenteral drug delivery system should be biocompatible and biodegradable, and the rate of biodegradation should be optimized according the administration frequency and drug release. PSi is generally recognized to be

biodegradable through hydrolytic degradation and dissolves into silicic acid, which is the naturally occurring form of Si in the body [18-21]. PSi is practically insoluble at low pH, but the dissolution of PSi increases at pH 7 and above, which means that PSi is soluble at physiological pH of 7.4 of s.c. tissue [22]. In addition, the surface modifications and porosity of PSi are known to affect the PSi dissolution rate *in vitro* and hence, the PSi residence time in the body can potentially be varied from hours to weeks and months [14,18,22].

The degradation and clearance studies regarding siliceous nanoparticles, including PSi, have been recently reviewed by Croissant et al. for more thorough overview of the factors, such as morphology, surface oxidation, functionalization and porosity, which have been found to affect the degradation mostly *in vitro*, with only limited number of *in vivo* reports describing PSi distribution or clearance after intravenous, intratumoral or retro-orbital administration [21].

When foreign material is being introduced into the body, it might induce a massive inflammatory reaction and formation of a fibrous capsule surrounding the material, which is definitely an unwanted phenomenon for a drug delivery system. Thermally oxidized PSi (TOPSi) and thermally carbonized PSi (TCPSi) were well tolerated by human corneal and epithelial cells and very little host reaction was elicited after implantation of TOPSi membranes into the rat eye [19,23]. The local injection of hydrophobic THCPSi microparticles (7 and 19 µm in diameter) into rat heart caused a transient activation of proinflammatory cytokine and fibrosis promoting genes, which was not observed after injection of hydrophilic TOPSi [24]. We have earlier shown that single s.c. injection of thermally hydrocarbonized (THCPSi) microparticles (38-56 µm) did not cause major inflammatory responses, but inflammatory and cytotoxic response to s.c. THCPSi implants (5x5x2 mm^3), developed for biosensing purposes, were shown to be due to reactive oxygen species in mice [4,25]. Since the biocompatibility is affected by the particle size and surface

chemistry, it should be evaluated with the PSi sample of interest when developing novel delivery systems [26-28].

The *in vivo* PSi biodegradation or PSi particle morphology has not been investigated after s.c. delivery [21]. Even though biodegradability of PSi is very well recognized, it is not known how the *in vivo* biodegradation takes place; from where the dissolution of PSi initiates or disintegration of the particles occurs. These gaps in the knowledge hinder the development of PSi based s.c. delivery systems for long-term use and the knowledge would be beneficial for other biomedical purposes as well. Therefore, the present study was carried out to evaluate the PSi biodegradation after s.c. administration in mice. Thermally oxidized, thermally carbonized and carboxylated thermally hydrocarbonized PSi (TOPSi, TCPSi and UnTHCPSi, respectively), were investigated for their biodegradation *in vivo* and solubility *in vitro*. These PSi samples, which differ from each other only by their surface chemistry, were analyzed utilizing micro-computed tomography (μCT), transmission electron microscopy (TEM) and X-ray diffraction (XRD). In addition, to evaluate the biocompatibility, the histopathology of the s.c. injection site was investigated.

2. MATERIALS AND METHODS

2.1 Reagents

Si wafers, p+ type (100) with resistivity of 0.01–0.02 Ωm were donated by Okmetic Finland for preparing the PSi samples. Hydrofluoric acid (HF) was bought from Merck Germany and ethanol (EtOH, 99.5%) from Altia (Helsinki, Finland). Phosphate-buffered saline (pH 7.4 PBS, Dulbecco's phosphate buffered saline 10x, Sigma-Aldrich, St. Louis, MO, USA) was diluted with Milli-Q water and used as a buffer in the *in vitro* solubility experiments. Sodium chloride solution (9 mg/ml) for s.c. injections was obtained from B. Braun Melsungen AG (Melsungen, Germany). Acrylic glue (Loctite Super Glue Precision, Henkel Norden Ab,

Sweden) was utilized in preparation of the s.c. tissue samples for micro-computed tomography (μCT). Hexamethyldisilazane (HMDS) and neutral buffered 10% formalin solution were purchased from Sigma-Aldrich (St. Louis, MO, USA). Glutaraldehyde solution and osmium tetroxide were purchased from Electron Microscopy Sciences (PA, USA) and LX-112 resin from Ladd Research Industries, Inc (VT, USA) for tissue transmission electron microscopy. The calibration standards for the Si determination of the *in vitro* samples were prepared using traceable 1000 mg L^{-1} single element stock solution (Titrisol) obtained from Merck (Darmstadt, Germany). In addition, nitric acid (67-69%, Romil, SpA) was used for the acidification of the standards and samples. The reagents used for tissue staining were Dakon Hematoxylin (REF CS700), Dakon Eosin (REF CS 701) and Dakon Bluing Buffer (REF CS702) (Agilent technologies, USA).

2.2 Animals

The C57Bl6/6NCrl male mice (26.4±2 g) were purchased from Laboratory Animal Center of the University of Oulu, Finland. The mice were housed in an environment controlled room with a 12 h light rhythm, with lights on at 6 am. The mice were fed *ad libitum* with commercial rodent chow (Teklad Global Rodent Diet T.2018C.12, Harlan Teklad, USA) and tap water was freely available throughout the experiment. The *in vivo* experiments were approved by the National Animal Experiment Board and conducted following the guidelines based on the EU Directive 2010/63/EU for animal experiments and National Act (497/2013) and Decree (564/2013) on the protection of animals used for scientific or educational purposes.

2.3 PSi particle fabrication

Free-standing PSi films were etched on Si wafers using 1:1 (39% HF: 99.5% EtOH) electrolyte, 50 mA/cm^2 current density and 40 min etching time. The freestanding films were milled into microparticles and sieved into 38–150 μm size fraction. The particles were briefly

treated with the electrolyte to replace the surface oxides with hydrogen terminated Si species and dried at 65 °C for 2 h. The particles were divided into three batches for surface modification. Oxidation was performed in air at 700 °C for 7.5 min [29]. Thermal carbonization was performed in two step process at 500 °C and 820 °C [30]. UnTHC surface modification consisted of thermal hydrocarbonization at 500 °C followed by undecylenic acid functionalization [10]. Subsequently, the surface modified particles were sieved into 53–75 µm size fraction first by dry sieving followed by wet sieving with ethanol and dried at 65 °C for 2 h. The particle size was chosen to meet the resolution limits of the µCT-scanner during the long term *in vivo* experiment, based on the results from a preliminary study. Finally, the particles were sterilized for *in vivo* use by heating at 180 °C for 30 min according the World health organization recommendations for dry heat sterilization [31].

2.4 PSi particle characterization

Laser diffraction measurements for particle size distribution was carried out with Malvern Mastersizer 2000 (UK). The samples were measured in water suspensions, except for UnTHCPSi particles which were suspended in ethanol because of their hydrophobicity.

Nitrogen ad/desorption measurements were done with Micromeritics Tristar II 3020 instrument (USA). The surface area was calculated with BET theory and pore size with BJH theory from the desorption branch [32,33]. Pore volume was calculated from a single point at 0.98 relative pressure.

Contact angle was measured by applying a droplet of de-ionized water on UnTHCPSi powder bed and determining the contact angle from a photograph. The droplet fully wetted the TOPSi and TCPSi powders because of their hydrophilicity and contact angle could not be determined.

Thermogravimetric (TG) analysis was performed with TA Q50 instrument (USA) in nitrogen atmosphere to analyze the undecylenic acid content in the UnTHCPSi particles. The experiments were done from 40 °C to 700 °C with a heating rate of 20 °C/min.

To analyze the surface modifications, FTIR measurements were performed with Thermo Scientific Nicolet 8700 (USA) using ATR (attenuated total reflectance) sample holder. The spectral range was 500−4000 cm^{-1} and resolution 4 cm^{-1}.

Morphology of the freshly prepared particles was characterized with scanning electron microscope (SEM, Zeiss Sigma HD). Acceleration voltage of 5 kV was utilized with secondary electron detector or InLens detector (high resolution).

2.5 In vitro dissolution of PSi particles

To evaluate the degradation of the PSi samples *in vitro,* the dissolution of PSi with different surface chemistries in a physiological buffer was studied. The PSi samples were weighed and placed into polypropylene tubes in pH 7.4 PBS buffer, with mild agitation in a water bath. The temperature of the water bath was set to 34 ˚C, since it represents the temperature in the s.c. tissue [2]. The PSi particle concentration was 0.05 mg/ml in the buffer, and hence the Si solubility (0.12 mg/ml) did not limit the PSi dissolution. At fixed time points (1, 2, 3, 5, 7 and 14 days for TOPSi and 1, 7, 14, 21, 28 and 56 days for TCPSi and UnTHCPSi samples) the tubes were removed from the water bath and 1.5 ml (V_{tot} 20 ml) samples were withdrawn and stored at -70˚C for later Si analysis.

2.6 Si analysis

The samples collected from the PSi *in vitro* buffer were analysed for their Si content using inductively coupled plasma optical emission spectroscopy (ICP-OES). Agilent 5100 SVDV ICP-OES (Agilent Technologies) equipped with inert sample introduction system was used in

the determination of Si (251.611 nm). Prior to the ICP-OES determination, the samples were diluted to the selected calibration range (0.1–2 mg L^{-1}) using 2% (v/v) nitric acid.

2.7 Exposure of the PSi samples to subcutaneous tissue in vivo

At the beginning of the experiment, the mice (n=46) were divided into 4 groups to receive one of the following samples as s.c. injections: a) TOPSi, b) TCPSi, c) UnTHCPSi or d) control. The mice were injected into their backs with either 2 mg of PSi microparticles (2 mg PSi in 200 µl NaCl 0.9%, n=3) bilaterally or NaCl 0.9% (200 µl, n=2) as control injections. The TOPSi samples were collected at days: 1, 2, 3, 5 and 7 after the injections, due to the faster biodegradation compared with the other investigated PSi types, as was observed in preliminary studies. TCPSi and UnTHCPSi samples were collected at 1, 7, 21 and 56 days after the s.c. injections.

Prior the sample collection, the mice were humanely killed using CO_2. The fur was removed and the injection sites were identified by dissecting the back of the mice. One PSi sample site, from the bilateral injections, was used for collecting the samples for transmission electron microscopy (TEM) and histopathology and the other for µCT-scanning and XRD analysis.

2.8 Histopathology of the subcutaneous injection site

For the histopathology, the tissue samples from the injection sites were fixed with 10% neutral buffered formalin solution, embedded with paraffin and cut into 5 µm sections for hematoxylin and eosin staining (HE). As a control, the mice received as an s.c. injection corresponding volumes of 0.9% NaCl, without PSi. The presence of inflammatory cells; monocytes, neutrophilic and eosinophilic granulocytes and lymphocytes was recorded. In addition, the location of the PSi particles, presence of giant cell reaction, and granulomatous inflammation were evaluated. The degree of inflammation was scored 0, 1, 2 and 3, corresponding to no inflammation, mild, moderate and severe inflammation, respectively (Figure S3, supplementary data).

2.9 Transmission electron microscopy (TEM)

Thin slices of s.c. tissues with PSi particles, harvested from the mice and stored in ethanol, were investigated with TEM. Before the analysis, samples were pre-fixed with 2.5% glutaraldehyde solution (phosphate buffered, pH 7.4) and post-fixed with 1% osmium tetroxide solution (phosphate buffered, pH 7.4) to prevent degradation of residual biological tissues. Afterwards, the samples were dehydrated by gradually changing the buffer solution to ethanol and dried subsequently. The samples were embedded with LX-112 resin polymerized at 60 °C for two days. The cast samples were then cut with microtome (Leica EM UC7, Diatome diamond knife ultra 45°) to ca. 70 nm slices and imaged with JEOL JEM 2100F instrument with 200 kV voltage.

2.10 Micro-computed tomography (µCT)

The s.c. tissue samples, containing PSi particles, were rolled to form small cylinders and closed with acrylic glue to facilitate the µCT-scanning of the samples. To dehydrate the tissue surrounding the PSi particles, the prepared samples were incubated for 2 hours in each of the following solutions: 70, 80 and 90% (overnight), 98% and 99.5% ethanol, followed with 2 h incubation in HMDS, immediately after sample collection. After the dehydration procedure, the samples were dried overnight at room temperature in a fume hood.

After the sample preparation, the tissue rolls were scanned with SkyScan1272 (Bruker microCT, Kontich, Belgium). An X-ray tube was set to 45kV and 0.25mm thick aluminum filtered was applied. Projection images with 1.5 um pixel size were collected every 0.2º over 360º with frame averaging of three. Image stacks were reconstructed using NRecon software (Bruker microCT, Kontich, Belgium) and both ring artifact and beam hardening corrections were applied to minimize these artifacts.

Images were analyzed with CTAnalyser (Bruker microCT, Kontich, Belgium). Particles were segmented in two phases since they were tightly packed. First a region of interest (ROI) mask

was produced by using global thresholding, despeckle and morphological operations. To segment individual particles inside ROI 3D unsharp mask with two pixel radius and adaptive thresholding (mean of min and max grey scale value) within 6 pixel radius were applied to original image stacks. This segmentation was cleaned with despeckle and the result was subjected to individual object analysis to calculate volume, sphericity, and average density for each particle [34].

2.11 X-ray diffraction (XRD)

Prior to the X-ray powder diffraction measurements, the PSi containing tissue samples from µCT scans were treated with liquid nitrogen and cut into thin sections and set on a zero-background sample holder. Reference PSi particles were measured on a zero-background sample holder as such. The samples were measured with Bruker AXS D8 Discover-diffractometer (Lynxeye 1D-linear detector), utilizing Bragg-Brentano reflection geometry. The angular range was 25–60° with a step size of 0.041° 2θ. On the primary side a 2.5° axial soller and on the secondary side 3° antiscatter slits were used. On the primary side a motorized divergent slit was used to radiate the sample length of 13 mm. Copper X-ray tube was used and the Kβ radiation was removed with a 0.02 mm Ni-filter. The measurement time was 60 min.

The obtained data was analyzed with TOPAS 4.2 software. For the measured diffractograms, whole profile fitting was done with Pawley method. For the profile fitting purposes, the required broadening caused by the instrument was analyzed using the diffractogram of Corundum-standard with whole profile fitting. The background was evaluated using Chebychev-polynoms and the lowest possible value was selected, which matched well the diffractogram. Peak broadenings were analysed with the integral breadth method and TOPAS software analyzed the errors.

2.12 Statistical analysis

The results from the *in vitro* dissolution experiment were tested for their statistical significance using 2-way Anova and Sidak's multiple comparisons tests (Graph Pad Prism 7.02, GraphPad Software Inc, CA, USA). The degree of inflammation was tested using One-way Anova followed by Tukey's post hoc test (SPSS Statistics). The differences between the *in vivo* TCPSi and UnTHCPSi samples were analyzed using multiple t-test followed with Holm-Sidak method. The differences within one *in vivo* PSi sample were tested with t-test. The level of statistical significance was set at $p<0.05$.

3. RESULTS

3.1 Particle characterization

The prepared PSi samples, TOPSi, TCPSi and UnTHCPSi were characterized with laser diffraction for particle sizes, nitrogen ad/desorption for porous properties, contact angle for hydrophobicity, FTIR for surface chemistry (supplementary data, S1) and SEM for particle morphology. The SEM micrographs demonstrate the irregular particle shape and porous surface of all the PSi samples (Figure 1). The results from the particle characterization are summarized in Table 1. TG analysis was applied to analyze the mass fraction of the undecylenic acid conjugated to the UnTHCPSi particles, which was 1.5±0.3% w/w corresponding to the surface density of 0.15 molecules/nm^2. In the calculation, 184.27 g/mol was taken as the molecular weight of undecylenic acid, and 322 m^2/g as the surface area of UnTHCPSi (Table 1).

3.2 In vitro dissolution of PSi particles

The PSi samples were placed into PBS buffer at 34˚C (pH 7.4) and the Si content of the buffer was analyzed at fixed time points. The measured Si concentrations are presented in Figure 2. PSi particle concentration was 0.05 mg/ml, which is lower than the solubility of Si from SiO_2 (0.12 mg/ml), and hence ensured that buffer saturation did not limit the dissolution of PSi.

The surface chemistry of the PSi samples affected significantly their dissolution. After one week, the Si concentration of the TOPSi sample was remarkably higher, compared with the other PSi samples (Figure 2). The final Si concentration after the 14 days' incubation was 28.6±6.0 mg/l, but the particles could not be visually observed anymore after 10 days. In contrast, after 56 days, some TCPSi particles were still present in the buffer and the Si concentration was 31.8±5.4 mg/ml. The Si concentration curve of the buffer shows that the dissolution of TCPSi occurred mainly between 28 and 56 days (Figure 2). After 28 days, the difference between the Si concentrations of TCPSi and UnTHCPSi buffers became statistically significant. Compared with the other PSi samples, UnTHCPSi remained nearly undissolved during the experiment, since the Si concentrations remained practically unaltered being <2 mg/l throughout the 56 days in the buffer. To summarize, the order of dissolution rate and extent *in vitro* were TOPSi>TCPSi>UnTHCPSi.

3.3 Biodegradation of the PSi particles in the subcutaneous tissue

To investigate the biodegradation of PSi, the samples were administered s.c. to mice and collected at predetermined time points to be examined with μCT, TEM and X-ray powder diffraction.

3.4 Transmission electron microscopy (TEM) analysis of the PSi samples

Individual particles, harvested from s.c. tissue, were evaluated with TEM to clarify the changes in the particle morphology during the *in vivo* experiment. Summaries of the obtained TEM micrographs are presented in Figs. 3, 4 and 5 for TOPSi, TCPSi and UnTHCPSi, respectively. In the images, differences in the spatial propagation of dissolution between the PSi samples can be observed. In the TOPSi samples (Figure 3, 1-7), the dissolution initiated from the external surface and on the pore walls resulting in collapse of the pore structure, irregular external surface and disintegration of the particles into smaller ones and the fastest degradation. In contrast, in the first time points, the external surface and pore structure in

TCPSi particles seem rather intact but some dissolved spots can be detected within the internal structure, which created defects on the regular porous structure (Figure 4-1). After three weeks in the s.c. tissue, the UnTHCPSi particles had remained mostly intact showing only slight traces of dissolution on the external surface of the particles. At the end of the experiment, also UnTHCPSi particles started to dissolve and degrade more throughout the pore structure, in a similar manner to TOPSi, which can be seen as irregularities on the PSi external and pore surfaces (Fig. 5).

3.5 Micro-computed tomography analysis of the PSi samples

The PSi samples collected from the s.c. space were imaged using an *ex vivo* μCT-scanner. Density index, sphericity and volume were calculated to clarify the 3D biodegradation of different PSi samples in the s.c. tissue.

The density of TOPSi and TCPSi decreased as a function of time (Figure 6). The density of TOPSi at five days was significantly lower ($p<0.05$) compared with the density at the beginning of the experiment. In a similar manner, the density of TCPSi was significantly lower ($p<0.001$) at the end of the experiment, than after the first day contact in the tissue. In contrast, density of UnTHCPSi remained stable through the experiment and these samples were significantly denser than TCPSi after 56 days contact with the s.c. tissue.

When the particle median volume was analyzed, the volume of TOPSi particles decreased gradually during the experiment (Figure 7) being over 50% smaller after 5 days, compared with the first sample. It must be noted that TOPSi particles could be detected only in one of the parallel samples a week after the injections. A decreasing trend can be seen also in the TCPSi sample (ca. 70% of the original volume at 56 days), whereas the volume of UnTHCPSi particles remained nearly unchanged throughout the experiment (ca. 95%). Sphericity of the PSi samples was analyzed to evaluate the change in the shape of the

irregularly shaped PSi particles during the experiment and the results showed no significant changes in the particle shape during the experiment (Figure S2, supplementary data), although a slight change towards more spherical shape was observed in TOPSi.

Figure 8 visualizes the PSi particles, collected from the s.c. tissue and prepared for *ex vivo* µ-CT scanning, at the beginning and at the end of the experiment. The particles appear in the figure as bright green higher contrast areas, which is surrounded by the s.c. tissue. The diameter of the prepared tissue sample was ca. 8 mm and the median particle size was ca. 80 µm (Table 1). Interestingly, there seemed to be a difference in the localization of the particles after the injections. The hydrophobic UnTHCPSi particles (right) were located in a denser manner, whereas hydrophilic TOPSi and TCPSi spread along the injection vehicle (Figure 8).

3.6 X-ray diffraction analysis of the PSi particle samples

The PSi samples were analyzed with XRD to evaluate their structure after contacting the s.c. tissue. According to the Babinet principle, PSi diffractogram can be assumed to be a superposition of two components; one representing the diffractogram of the solid Si particles and one similar to the diffractogram that would be obtained from Si structures with the shape identical to the pores [35].

When comparing the PSi samples, harvested from the s.c. tissue, with as prepared PSi particles, the diffraction peak positions were similar (28, 47 and 56 2θ°), indicative for Si. However, their intensities were markedly lower (Figure 9). This may be indicating loss of organized PSi structure, but the diffractograms may also be affected by the unequal amount of particles in the samples, collected from the s.c. tissue. The peak widths were analyzed in order to get information on the effect of the dissolution process on the pore structure. According to the Babinet principle and the Scherrer equation the peak width can be assumed

a measure of the pore size (here pore size equivalent) where narrower diffraction peak represents a larger pore size. It should be noted that the procedure used here is oversimplified and does not take into account e.g. the presence of the two components in the diffractograms mentioned above or presence of nanocrystallites broken off from the particles. Therefore, the results should not be considered as an accurate pore size, and the values given should not be directly compared with the values obtained from nitrogen ad/desorption, but we believe it still gives valuable information on the pore size development. When the pore size equivalents of the PSi samples were analyzed, a substantial increase can be seen in TOPSi particles during seven days, a moderate increase in the UnTHCPSi particles during 56 days, whereas the pore size remained unchanged in TCPSi (Table 2).

3.7 Histopathology

To evaluate the biocompatibility of the PSi samples in the s.c. tissue, the histopathology of the injection site was investigated (Figure 10). There were no statistically significant differences between the different PSi samples. After one day from the injections, signs from mild to moderate transient acute inflammation could be detected in the all PSi samples and the presence of inflammatory cells (monocytes, neutrophilic/eosinofilic granulocytes and lymphocytes) at the injection site decreased gradually after that (Table 3 and Supplementary data Table S2). After the TOPSi particle injections, signs of moderate and mild inflammation were detected until 5 and 7 days, respectively. Some infiltration of leukocytes towards the TOPSi and UnTHCPSi particles could be detected until 7 days after the injections. In the case of the TCPSi and UnTHCPSi particles, 21 days after the injections the inflammatory cells were completely absent. It must be noted that 7 days after the injections, some fibrosis was found to surround the particles in the TCPSi and UnTHCPSi samples. However, no signs of

giant cell reaction or granulomatous inflammation were observed in any of the samples, which would indicate severe foreign body reaction induced by the PSi samples.

4. DISCUSSION

TOPSi, TCPSi and UnTHCPSi samples were selected for the present study, because of their different surface properties and stability, to clarify the biodegradation of PSi at the actual administration site of s.c. delivery systems. It is known that the surface chemistry or other material characteristics of PSi affect the degradation and various protocols have been introduced to stabilize the fresh hydrogen terminated PSi surface, which is too unstable for many purposes [36,37]. It is also known that porosity and the specific surface area affect the degradation rate of PSi *in vitro* [18,38]. However, *in vivo* data describing PSi biodegradation is scarce and it is not known how the biodegradation process takes place within the PSi particles. As described earlier, s.c. tissue has its own characteristics as a route of administration. The biodegradation of PSi in the s.c. tissue has not been investigated earlier, even though it is important to clarify the biodegradation at the purported administration route, since it may have a significant effect on drug release. Therefore, various PSi samples were analyzed using TEM and XRD to clarify their biodegradation after s.c. tissue contact. In addition, density, volume and sphericity of the PSi particles were explored using μCT and solubility of the particles was confirmed *in vitro*.

All the investigated PSi microparticles were fabricated using ball-milling, which results in irregular particle morphology (Fig. 1). Due to the sieving process, the samples contained particles of various sizes, although the median sizes were the same. The degradation of Si particles is considered to be independent of the particle size, as long as the fabrication, porosity, surface area and other material parameters are comparable [21]. At the beginning of

the present study, the size, shape and morphology of the PSi particles were comparable (Table 1, Figure 1). However, it must be noted that the average pore diameter of TOPSi was about 10% larger compared with TCPSi and UnTHCPSi. This slight difference might also play a role in the biodegradation of TOPSi when compared with the other PSi samples, as the porosity is known to affect the dissolution rate [21]. The pore diameters of TCPSi and UnTHCPSi were within 0.5 nm, the latter having slightly smaller pores. Despite the slight difference in the porosity and its correlation with the biodegradation rates of the PSi samples, the surface modification is considered to be the most important factor controlling the dissolution of the PSi samples investigated in the present study.

TOPSi is hydrophilic with an oxidized surface. Another hydrophilic sample was TCPSi, which has chemically a very stable carbide surface. In contrast, UnTHCPSi particles were hydrophobic, with a surface covered by hydrocarbons and carboxylic groups. It must be noted that the PSi particle amounts, collected from the s.c. tissue, could not be directly compared, since some of the particles were lost during the sample collection.

In vitro, TOPSi particles dissolved completely in approximately 10–14 days, when no particles could be visually observed. TOPSi dissolved and disintegrated fastest also *in vivo*. The TOPSi particles could not be detected one week after the injections, with one exception, which was most likely due to excessive s.c. fat deposit around the TOPSi sample hindering their degradation. According the µCT data, the TOPSi particles lost over 10% of their initial density in one week. The volume of TOPSi particles decreased the most, compared with the other PSi particles, and these particles became more spherical in contact with the s.c. tissue, indicating degradation from the external surfaces (supplementary data, Figure S2). Supporting that, TEM micrographs demonstrated that the dissolution of TOPSi seemed to begin from the external surfaces of the microparticles. The pore size of TOPSi particles

increased as a function of time, as observed in the XRD studies, indicating that TOPSi dissolved also inside the pores i.e. from the pore walls.

At the end of the *in vitro* experiment (56 days), some of the TCPSi particles were still observed in the buffer. After 21 days, the Si concentrations of the TCPSi buffer increased significantly, indicating faster rate of dissolution (Figure 2). *In vivo*, dissolution of TCPSi particles was observed to be initiated locally inside the particles, as seen in TEM analysis (Figure 4). According the µ-CT data, the density of TCPSi decreased markedly during eight weeks, being significantly lower compared with UnTHCPSi at the end of the experiment (Figure 6). Also, the TCPSi particle volume lowered towards the end of the experiment (Figure 7). However, the pore sizes of the TCPSi particles remained similar throughout the experiment (Table 2). Based on these observations it seems that the biodegradation of TCPSi did not proceed through the carbide layer on the pore surfaces. Instead the biodegradation originated from the inner parts of the particle matrix (Figure 4) at points where the carbide coverage of TCPSi surface might not have been complete. After the initiation, the dissolution then most likely proceeded under the carbide layer covered surface, inside the pore walls, and caused the particle structure to erode.

The low Si concentrations of the *in vitro* buffer indicate that UnTHCPSi particles remained almost intact during the experiment (Figure 2) and TEM analysis showed no signs of UnTHCPSi biodegradation 7 days after the injections (Figure 5). A slight increase in the pore size was observed with XRD, which progressed as the study proceeded, being moderate after 56 days. When the UnTHCPSi samples were in contact with the s.c. tissue for longer periods, it was noted that the biodegradation started from the external surface, in a similar manner to TOPSi (Figure 5). However, the density and volume of UnTHCPSi particles remained the same during 56 days. It is likely that later on, also the density and volume would decrease.

To summarize, the order of *in vitro* solubility was TOPSi, followed by TCPSi and UnTHCPSi. The present data demonstrates TOPSi to have the fastest biodegradation rate also *in vivo* and its pore size increased, volume and density decreased as a function of time. In addition, the TOPSi particles seemed to degrade from the external and pore surfaces. Interestingly, the TCPSi particles started to degrade from the internal parts, and the pore size remained unaffected despite the decrease in the density. The biodegradation of UnTHCPSi proceeded in a similar manner with TOPSi, but with a much slower rate and without significant changes in the density or particle volume during this experiment. Unlike the other samples, the UnTHCPSi particles are hydrophobic, which affects their wettability by the surrounding interstitial liquid in s.c. tissue. After the injections, the distribution of UnTHCPSi was different from the hydrophilic TOPSi and TCPSi, as they located denser manner at the injection site, whereas the other PSi samples spread more within the suspension (Figure 8). This is perhaps due to the hydrophobic particles gathering closely in a hydrophilic environment, which further hinders the particle wetting and their dissolution. As the UnTHCPSi particles eventually will become properly in contact with the circulating aqueous solution, the stabilizing surface will most likely wear away first from the particle external surface, initiating the biodegradation, and later inside the pore surfaces. It is likely that the rate of UnTHCPSi biodegradation would increase finally when UnTHC surface stabilization wears off and enables the dissolution. However, more and longer investigations would be needed to address this issue.

In the present study, there were no signs of severe inflammation or foreign body reaction after s.c. administration of any the PSi samples, using relatively high dose of PSi (2 mg) particles. In general, PSi is known to be biocompatible *in vitro* and *in vivo*, which is depending on the surface chemistry, particle size and the concentration of PSi [11,28]. We have shown previously that s.c. injected THCPSi microparticles (38–53 µm) did not induce

massive cytokine release in mice [25]. After the administration, an acute inflammation lasted for few days, and was most likely due to tissue damage caused by the injection and introduction of the biomaterial for the biological system in general as no chronic inflammation was detected [39]. Surface properties of the s.c. delivered biomaterial, such as hydrophilicity or hydrophobicity, affect significantly whether it will induce a foreign body reaction, which may finally lead to a relatively fast fibrous capsule formation that might even prevent drug release to systemic circulation [40,41]. Hydrophilic TOPSi has hydroxyl groups on its surface, which have been found to promote fibrosis [39]. However, THCPSi nanoparticles have been shown to induce more fibrosis promoting genes compared with TOPSi micro- and nanoparticles in rat myocardium [24]. This difference may be due to the faster biodegradation of TOPSi, which attenuates the induction of fibrosis. In the present study, it was observed that more stable TCPSi and UnTHCPSi particles have a tendency to induce fibrosis around the particles after the acute inflammation is diminished. In a previous study, carboxylic acid groups on the surface of hydrophobic biomaterial, as is the case with UnTHCPSi, have shown induce fibrosis and even formation of a fibrotic capsule [39]. In the present study, no fibrotic capsule was detected around the PSi particles even after two-month period. In addition, because of the absence of foreign body giant cell formation with the PSi samples, the observed fibrosis may be due to normal wound healing process. However, when developing these materials further, more studies are needed to clarify how the fibrosis formation proceeds and whether it affects the further biodegradation of the slowly degrading PSi samples.

5. CONCLUSIONS

This was the first time, when *in vivo* PSi biodegradation was systemically investigated after s.c. administration. Several analytical techniques were utilized to analyze the particle

structure. Surface modification of PSi particles affected the biodegradation rate and spatial propagation of the dissolution.

TOPSi shows potential to serve as a delivery system for compounds, which would benefit from a maximum one week dosing interval. TCPSi and UnTHCPSi offer possibilities for lower administration frequency, ranging from weeks to several months. There are number of peptide drugs that would benefit from a delivery platform offering such wide-ranging biodegradation time frame. Altogether, the results reported here serve as an excellent basis for the further development of various PSi materials for s.c. drug delivery purposes and may be used for further formulation development for various peptides or other therapeutic compounds.

Acknowledgements and funding

The authors thank SIB Labs, University of Eastern Finland for providing laboratory facilities, Virpi Miettinen (UEF), Riitta Vuento (UO), Herkko Pulkkinen (UEF) for excellent technical support. Academy of Finland (#287625) and Finnish Cultural Foundation are acknowledged for funding (MK).

Conflict of interest

None.

References

[1] K. Fosgerau, T. Hoffmann, Peptide therapeutics: current status and future directions, Drug Discov. Today 20 (2015) 122-128.

[2] P. Webb, Temperatures of skin, subcutaneous tissue, muscle and core in resting men in cold, comfortable and hot conditions, Eur. J. Appl. Physiol. Occup. Physiol. 64 (1992) 471-476.

[3] M.P.A. Ferreira, S. Ranjan, A.M.R. Correia, E.M. Mäkilä, S.M. Kinnunen, H. Zhang, M. Shahbazi, P.V. Almeida, J.J. Salonen, H.J. Ruskoaho, A.J. Airaksinen, J.T. Hirvonen, H.A. Santos, In vitro and in vivo assessment of heart-homing porous silicon nanoparticles, Biomaterials 94 (2016) 93-104.

[4] W.Y. Tong, M.J. Sweetman, E.R. Marzouk, C. Fraser, T. Kuchel, N.H. Voelcker, Towards a subcutaneous optical biosensor based on thermally hydrocarbonised porous silicon, Biomaterials 74 (2016) 217-230.

[5] D. Liu, H. Zhang, E. Mäkilä, J. Fan, B. Herranz-Blanco, C. Wang, R. Rosa, A.J. Ribeiro, J. Salonen, J. Hirvonen, H.A. Santos, Microfluidic assisted one-step fabrication of porous silicon@acetalated dextran nanocomposites for precisely controlled combination chemotherapy, Biomaterials 39 (2015) 249-259.

[6] M. Ariza-Avidad, A. Nieto, A. Salinas-Castillo, L.F. Capitan-Vallvey, G.M. Miskelly, M.J. Sailor, Monitoring of degradation of porous silicon photonic crystals using digital photography, Nanoscale Res. Lett. 9 (2014) 410-276X-9-410. eCollection 2014.

[7] C. Wang, M.P. Sarparanta, E.M. Mäkilä, M.L.K. Hyvönen, P.M. Laakkonen, J.J. Salonen, J.T. Hirvonen, A.J. Airaksinen, H.A. Santos, Multifunctional porous silicon nanoparticles for cancer theranostics, Biomaterials 48 (2015) 108-118.

[8] J. Riikonen, A. Correia, M. Kovalainen, S. Näkki, M. Lehtonen, J. Leppänen, J. Rantanen, W. Xu, F. Araujo, J. Hirvonen, K. Järvinen, H.A. Santos, V.P. Lehto, Systematic in vitro and in vivo study on porous silicon to improve the oral bioavailability of celecoxib, Biomaterials 52 (2015) 44-55.

[9] M. Kovalainen, J. Monkäre, M. Kaasalainen, J. Riikonen, V.P. Lehto, J. Salonen, K.H. Herzig, K. Järvinen, Development of porous silicon nanocarriers for parenteral peptide delivery, Mol. Pharm. 10 (2013) 353-359.

[10] M. Kovalainen, J. Mönkäre, E. Mäkilä, J. Salonen, V. Lehto, K. Herzig, K. Järvinen, Mesoporous silicon (PSi) for sustained peptide delivery: effect of PSi microparticle surface chemistry on Peptide YY3-36 release, Pharm. Res. 29 (2012) 837-846.

[11] M. Kovalainen, J. Mönkare, J. Riikonen, U. Pesonen, M. Vlasova, J. Salonen, V.P. Lehto, K. Järvinen, K.H. Herzig, Novel delivery systems for improving the clinical use of peptides, Pharmacol. Rev. 67 (2015) 541-561.

[12] M. Kilpeläinen, J. Mönkäre, M.A. Vlasova, J. Riikonen, V.P. Lehto, J. Salonen, K. Järvinen, K.H. Herzig, Nanostructured porous silicon microparticles enable sustained peptide (Melanotan II) delivery, Eur. J. Pharm. Biopharm. 77 (2011) 20-25.

[13] E. Tasciotti, X. Liu, R. Bhavane, K. Plant, A.D. Leonard, B.K. Price, M.M. Cheng, P. Decuzzi, J.M. Tour, F. Robertson, M. Ferrari, Mesoporous silicon particles as a multistage delivery system for imaging and therapeutic applications, Nat. Nanotechnol 3 (2008) 151-157.

[14] K.L. Jarvis, T.J. Barnes, C.A. Prestidge, Surface chemistry of porous silicon and implications for drug encapsulation and delivery applications, Adv. Colloid Interface Sci. 175 (2012) 25-38.

[15] S.V. Fulzele, P.M. Satturwar, A.K. Dorle, Study of the biodegradation and in vivo biocompatibility of novel biomaterials, Eur. J. Pharm. Sci. 20 (2003) 53-61.

[16] S.V. Fulzele, P.M. Satturwar, A.K. Dorle, Novel biopolymers as implant matrix for the delivery of ciprofloxacin: biocompatibility, degradation, and in vitro antibiotic release, J. Pharm. Sci. 96 (2007) 132-144.

[17] M. Kaasalainen, J. Rytkönen, E. Mäkilä, A. Närvänen, J. Salonen, Electrostatic interaction on loading of therapeutic peptide GLP-1 into porous silicon nanoparticles, Langmuir 31 (2015) 1722-1729.

[18] S.H.C. Anderson, H. Elliott, D.J. Wallis, L.T. Canham, J.J. Powell, Dissolution of different forms of partially porous silicon wafers under simulated physiological condotions, Phys. Stat. Sol. (a) 197 (2003) 331-335.

[19] S.P. Low, N.H. Voelcker, L.T. Canham, K.A. Williams, The biocompatibility of porous silicon in tissues of the eye, Biomaterials 30 (2009) 2873-2880.

[20] T. Tanaka, B. Godin, R. Bhavane, R. Nieves-Alicea, J. Gu, X. Liu, C. Chiappini, J.R. Fakhoury, S. Amra, A. Ewing, Q. Li, I.J. Fidler, M. Ferrari, In vivo evaluation of safety of nanoporous silicon carriers following single and multiple dose intravenous administrations in mice, Int. J. Pharm. 402 (2010) 190-197.

[21] J.G. Croissant, Y. Fatieiev, N.M. Khashab, Degradability and Clearance of Silicon, Organosilica, Silsesquioxane, Silica Mixed Oxide, and Mesoporous Silica Nanoparticles, Adv Mater 29 (2017) 1604634-n/a.

[22] S. Näkki, J. Rytkönen, T. Nissinen, C. Florea, J. Riikonen, P. Ek, H. Zhang, H.A. Santos, A. Närvänen, W. Xu, V.P. Lehto, Improved stability and biocompatibility of nanostructured silicon drug carrier for intravenous administration, Acta Biomater. 13 (2015) 207-215.

[23] E. Korhonen, S. Rönkkö, S. Hillebrand, J. Riikonen, W. Xu, K. Järvinen, V. Lehto, A. Kauppinen, Cytotoxicity assessment of porous silicon microparticles for ocular drug delivery, European Journal of Pharmaceutics and Biopharmaceutics 100 (2016) 1-8.

[24] M.A. Tolli, M.P. Ferreira, S.M. Kinnunen, J. Rysä, E.M. Mäkilä, Z. Szabo, R.E. Serpi, P.J. Ohukainen, M.J. Valimaki, A.M. Correia, J.J. Salonen, J.T. Hirvonen, H.J. Ruskoaho, H.A. Santos, In vivo biocompatibility of porous silicon biomaterials for drug delivery to the heart, Biomaterials 35 (2014) 8394-8405.

[25] M. Kilpeläinen, J. Riikonen, M.A. Vlasova, A. Huotari, V.P. Lehto, J. Salonen, K.H. Herzig, K. Jarvinen, In vivo delivery of a peptide, ghrelin antagonist, with mesoporous silicon microparticles, J. Control. Release 137 (2009) 166-170.

[26] L.M. Bimbo, M. Sarparanta, H.A. Santos, A.J. Airaksinen, E. Mäkilä, T. Laaksonen, L. Peltonen, V.P. Lehto, J. Hirvonen, J. Salonen, Biocompatibility of thermally hydrocarbonized porous silicon nanoparticles and their biodistribution in rats, ACS Nano 4 (2010) 3023-3032.

[27] L.M. Bimbo, M. Sarparanta, E. Mäkilä, T. Laaksonen, P. Laaksonen, J. Salonen, M.B. Linder, J. Hirvonen, A.J. Airaksinen, H.A. Santos, Cellular interactions of surface modified nanoporous silicon particles, Nanoscale 4 (2012) 3184-3192.

[28] H. Jaganathan, B. Godin, Biocompatibility assessment of Si-based nano- and micro-particles, Adv. Drug Deliv. Rev. 64 (2012) 1800-1819.

[29] J. Riikonen, M. Salomäki, J. van Wonderen, M. Kemell, W. Xu, O. Korhonen, M. Ritala, F. MacMillan, J. Salonen, V. Lehto, Surface Chemistry, Reactivity, and Pore Structure of Porous Silicon Oxidized by Various Methods, Langmuir 28 (2012) 10573-10583.

[30] J. Riikonen, E. Mäkilä, J. Salonen, V. Lehto, Determination of the Physical State of Drug Molecules in Mesoporous Silicon with Different Surface Chemistries RID A-6217-2010, Langmuir 25 (2009) 6137-6142.

[31] WHO, The International Pharmacopoeia - Sixth Edition, 2016. 5.8 Methods of sterilization. (2016).

[32] S. Brunauer, P. Emmett, E. Teller, Adsorption of Gases in Multimolecular Layers, J. Am. Chem. Soc 60 (1938) 309-319.

[33] E.P. Barrett, L.G. Joyner, P.P. Halenda, The Determination of Pore Volume and Area Distributions in Porous Substances. I. Computations from Nitrogen Isotherms., J. Am. Chem. Soc. 73 (1951) 373-380.

[34] H. Wadell, Volume, Shape, and Roundness of Quartz Particles, J. Geol. 43 (1935) 250-280.

[35] A. Bensaid, G. Patrat, M. Brunel, F. de Bergevin, R. Hérino, Characterization of porous silicon layers by grazing- incidence X-ray fluorescence and diffraction, Solid State Communications 79 (1991) 923-928.

[36] N.K. Hon, Z. Shaposhnik, E.D. Diebold, F. Tamanoi, B. Jalali, Tailoring the biodegradability of porous silicon nanoparticles, J. Biomed. Mater. Res. A. (2012).

[37] E.J. Anglin, L. Cheng, W.R. Freeman, M.J. Sailor, Porous silicon in drug delivery devices and materials, Adv. Drug Deliv. Rev. 60 (2008) 1266-1277.

[38] J. Peckham, G.T. Andrews, Comparative study of the biodegradability of porous silicon films in simulated body fluid, Biomed. Mater. Eng. 25 (2015) 111-116.

[39] R. Klopfleisch, F. Jung, The pathology of the foreign body reaction against biomaterials, J. Biomed. Mater. Res. A. (2016).

[40] J.M. Anderson, A. Rodriguez, D.T. Chang, Foreign body reaction to biomaterials, Semin. Immunol. 20 (2008) 86-100.

[41] S.S. Iyer, W.H. Barr, H.T. Karnes, Profiling in vitro drug release from subcutaneous implants: a review of current status and potential implications on drug product development, Biopharm. Drug Dispos. 27 (2006) 157-170.

Figure 1.

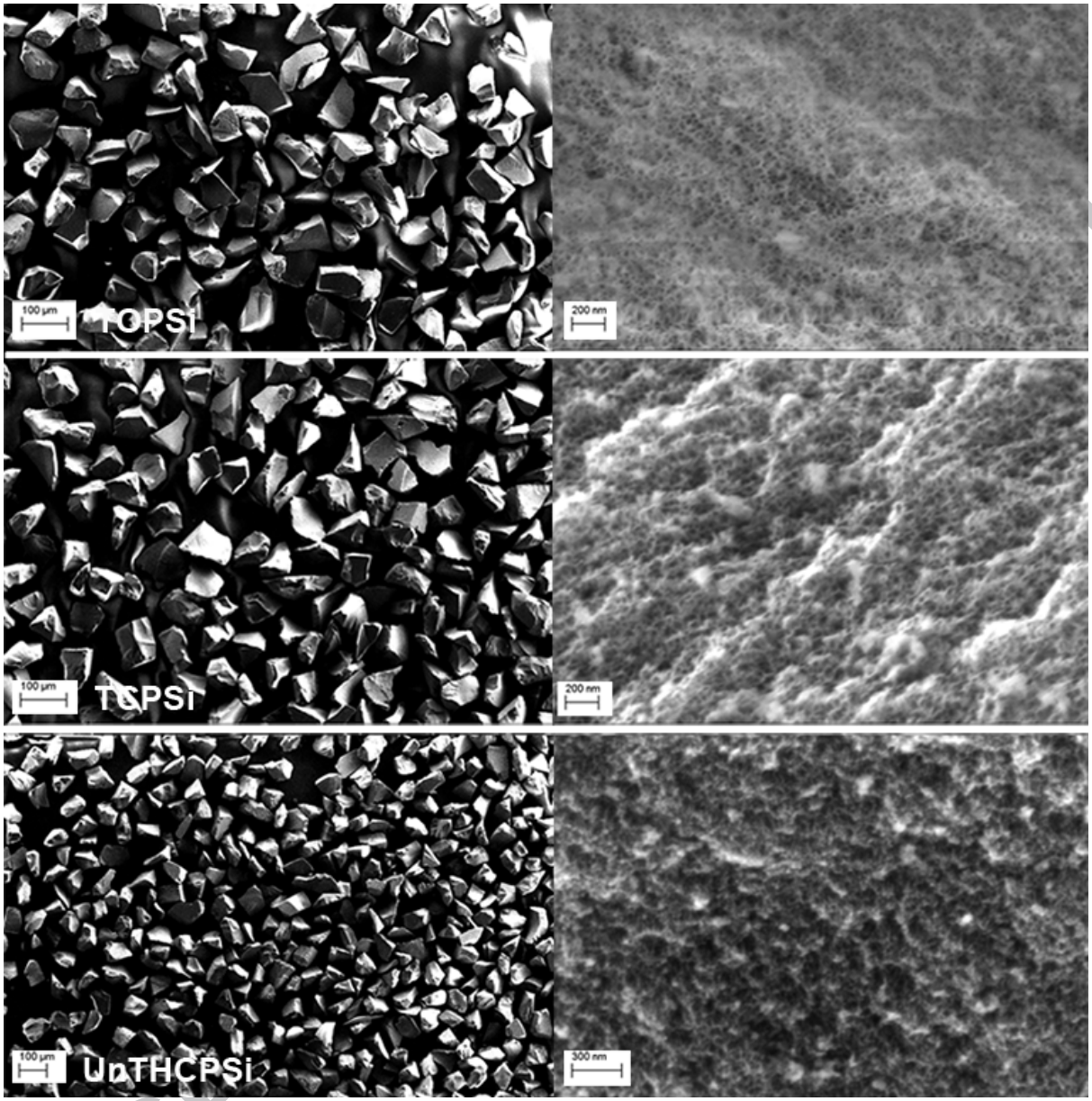
100 µm
TOPSi
200 nm
100 µm
TCPSi
200 nm
100 µm
UnTHCPSi
300 nm

Figure captions

Figure 1A. Morphology of irregularly shaped TOPSi (up), TCPSi (middle) and UnTHCPSi (below) microparticles (left) and their porous surfaces (right) after their fabrication. Note the difference in the scale bar of the SEM micrographs.

Figure 1B. Detailed structure of fresh PSi microparticles, visualized with TEM. TOPSi (up), TCPSi (middle) and UnTHCPSi (below).

Figure 2. The PSi surface chemistry affected significantly the dissolution rate and extent. The graph presents Si concentrations of the *in vitro* buffer (PBS, pH 7.4, 34 ˚C, n=3, mean±SEM), where the PSi samples were incubated. The Si concentration of buffer with TOPSi was significantly different from the other samples after 7 and 14 days (vs TCPSi **p<0.01 and vs UnTHCPSi ***p<0.001, @14 days ****p<0.0001) and TCPSi was significantly different compared with UnTHCPSi after 28 days (*p<0.05 and ****p<0.0001). The TOPSi particles could not be visually detected after 10 days and the data collection was terminated at 14 days.

Figure 3. TOPSi microparticles were harvested from s.c. tissue and evaluated with TEM 1, 2, 3, 5 and 7 days after the s.c. injections. The particles began to degrade from the external and pore surfaces, which can be observed in the summary of the TEM micrographs of individual particles. The degradation changes the external surface towards less intact and unstructured morphology.

Figure 4. TCPSi microparticles were harvested from s.c. tissue and evaluated with TEM 1, 7, 21 and 56 days after the s.c. injections. Degradation of the particles initiated locally inside the

particle matrix, which can be observed in the summary of TEM micrographs of individual particles. The degraded spots, where the degradation initiated, are seen as hollow space inside the particles.

Figure 5. UnTHCPSi microparticles were harvested from s.c. tissue and evaluated with TEM 1, 7, 21 and 56 days after the s.c. injections. The particles started to degrade slowly from the external surfaces, in a similar manner than faster degrading TOPSi microparticles (Fig. 3), which can be observed in the summary of TEM micrographs of individual particles.

Figure 6. The change of density of PSi particles after being in contact with s.c. tissue. The density of TCPSi sample was significantly lower compared with UnTHCPSi at 56 days (***$p<0.001$), TOPSi (*$p<0.05$) and TCPSi (+++$p<0.001$) particles had significantly lower densities after 5 and 56 days compared with the beginning of the experiment, respectively. The TOPSi samples were not collected after 7 days due to their faster degradation. (Mean±SEM, n=3, except TOPSi@day 7 n=1)

Figure 7. Median particle volume (Mean±SEM, n=3, except TOPSi@day 7 n=1). The volume of TCPSi particles was significantly lower at day 21 compared with UnTHCPSi particles ($p<0.001$). The TOPSi samples were not collected after 7 days due to their faster degradation.

Figure 8. Summary of the first (top row) and last (bottom row) collected PSi samples after contacting the subcutaneous tissue for 1 and 7 (TOPSi) or 1 and 56 (TCPSi and UnTHCPSi) days. The TOPSi samples were not collected after 7 days due to their faster degradation. The PSi particles appear in the picture bright, higher contrast areas in the middle of the samples (indicated by arrows) and are surrounded by the s.c. tissue. From these 3D visualizations it is

evident that UnTHCPSi particles were located in a denser manner, whereas hydrophilic TOPSi and TCPSi particles spread along with the injection vehicle.

Figure 9. X-ray diffractograms of the TOPSi, TCPSi and UnTHCPSi samples, collected from the s.c. tissue and the reference particles on the upper left panel. The reference shows the peak spectra of PSi and all the samples have corresponding peak positions of Si. However, the intensities and peak widths are different, indicating differences in the porous structure.

Figure 10. PSi microparticles in the hematoxylin-eosin stained subcutaneous tissue: A) TOPSi 1 day, B) TOPSi 7 days, C) TCPSi 1 day, D) TCPSi 56 days, E) UnTHCPSi 1 day and F) UnTHCPSi 56 days after the injections. Inflammatory cells were present in the s.c. tissue after injection of PSi samples. The number of inflammatory cells, monocytes, lymphocytes/plasma cells, neutrophilic and eosinophilic granulocytes decreased gradually after the injections and were completely absent after 21 days from the injections (D, F). No signs of chronic inflammation were observed.

Tables and headings

Table 1. Results from nitrogen ad/desorption, laser diffraction and contact angle determination of PSi powder (Mean ± SD, 3 measurements).

PSi sample	**Area (m^2/g)**	**Volume (cm^3/g)**	**Pore average diameter (nm)**	**Volume average diameter, *D*[4,3] (µm)**	**Particle median diameter (µm)**	**Contact angle (°)**
TOPSi	264±2	1.18±0.01	15.57±0.04	82.1±0.3	79.7±0.3	nd*
TCPSi	305±9	1.12±0.02	14.18±0.07	80.7±0.3	78.3±0.3	nd*
UnTHCPSi	322±5	1.17±0.01	13.8±0.2	81.9±0.4	79.5±0.4	116±9

*Because of the hydrophilicity of the samples, water wetted the powder bed and contact angle could not be determined.

Table 2. Pore size analysis using XRD. Mean±SEM, n=3 except TOPSi@day 7 n=1. na: not analyzed due to the experimental protocol.

	Pore size equivalent (nm)							
PSi samples	**Ref.**	**1 day**	**2 days**	**3 days**	**5 days**	**7 days**	**21 days**	**56 days**
TOPSi	10.2±0.2	12±1	11±2	11±2	14±4	40±30	na	na
TCPSi	10.1±0.2	10.1±0.3	na	na	na	12±3	10±1	11±1
UnTHCPSi	12.3±0.3	10.8±0.6	na	na	na	16±5	15±4	18±5

Table 3. Summary of the histopathological findings from the subcutaneous injection site of the PSi samples (inflammation range 0-3, n=3, na= not analyzed due to the sampling schedule, n=3 except TOPSi@day 7 n=1).

PSi sample / Days after injections	**Inflammation** (0=No; 1=mild; 2=Moderate; 3=severe)							**Fibrosis formation (+/-)**						
	1	**2**	**3**	**5**	**7**	**21**	**56**	**1**	**2**	**3**	**5**	**7**	**21**	**56**
TOPSi	0-2	1-2	1	1-2	0-1	na	na	-	-	-	-	+	na	na
TCPSi	0-2	na	na	na	0-1	0	0	-	na	na	na	+	+	+
UnTHCPSi	1-2	na	na	na	0-1	0	0	-	na	na	na	+	+	+
Control	0	0	0	0	0	0	0	-	-	-	-	-	-	-

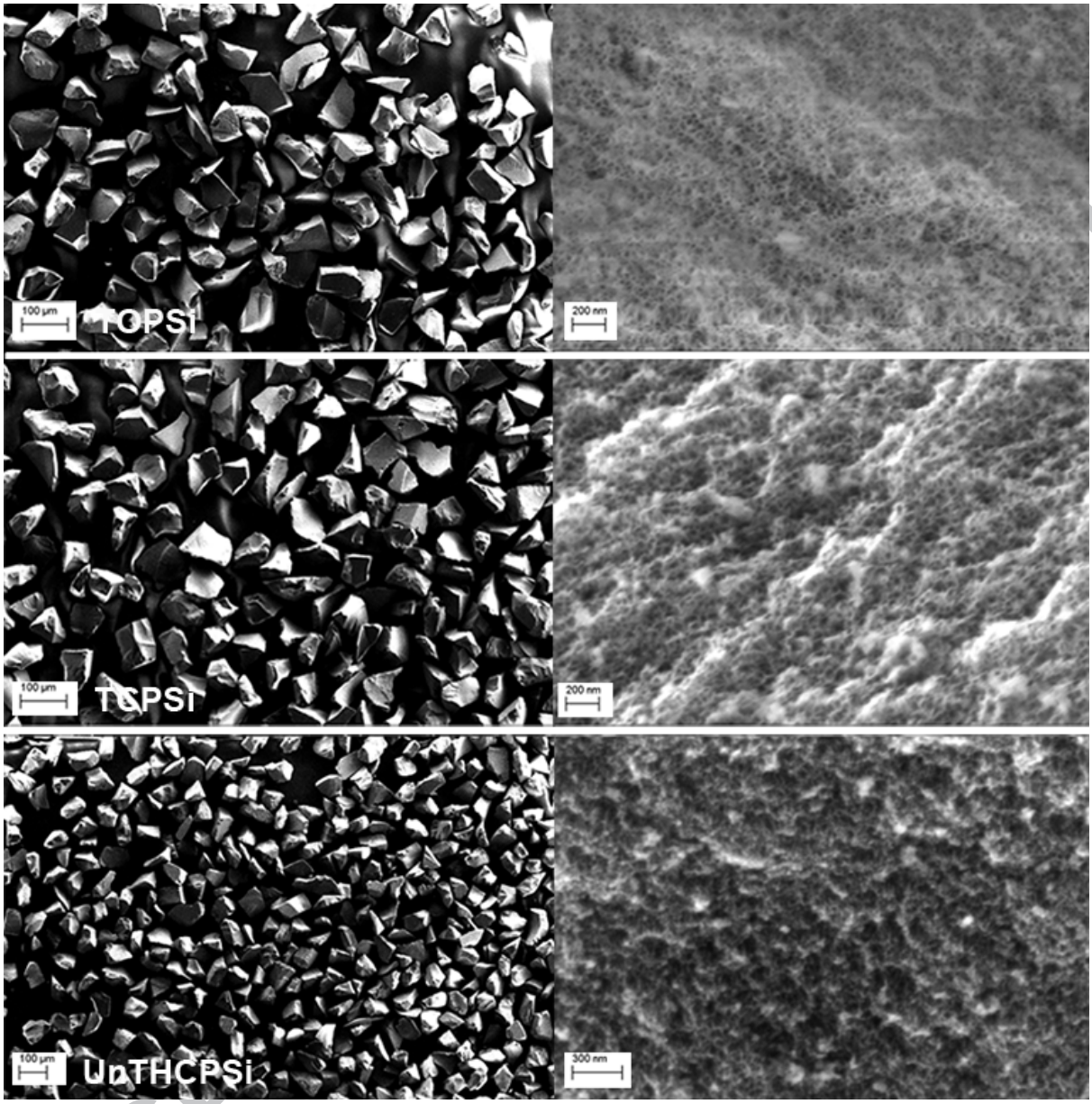
100 µm
TOPSi
200 nm
100 µm
TGPSi
200 nm
100 µm
UnTHCPSi
300 nm

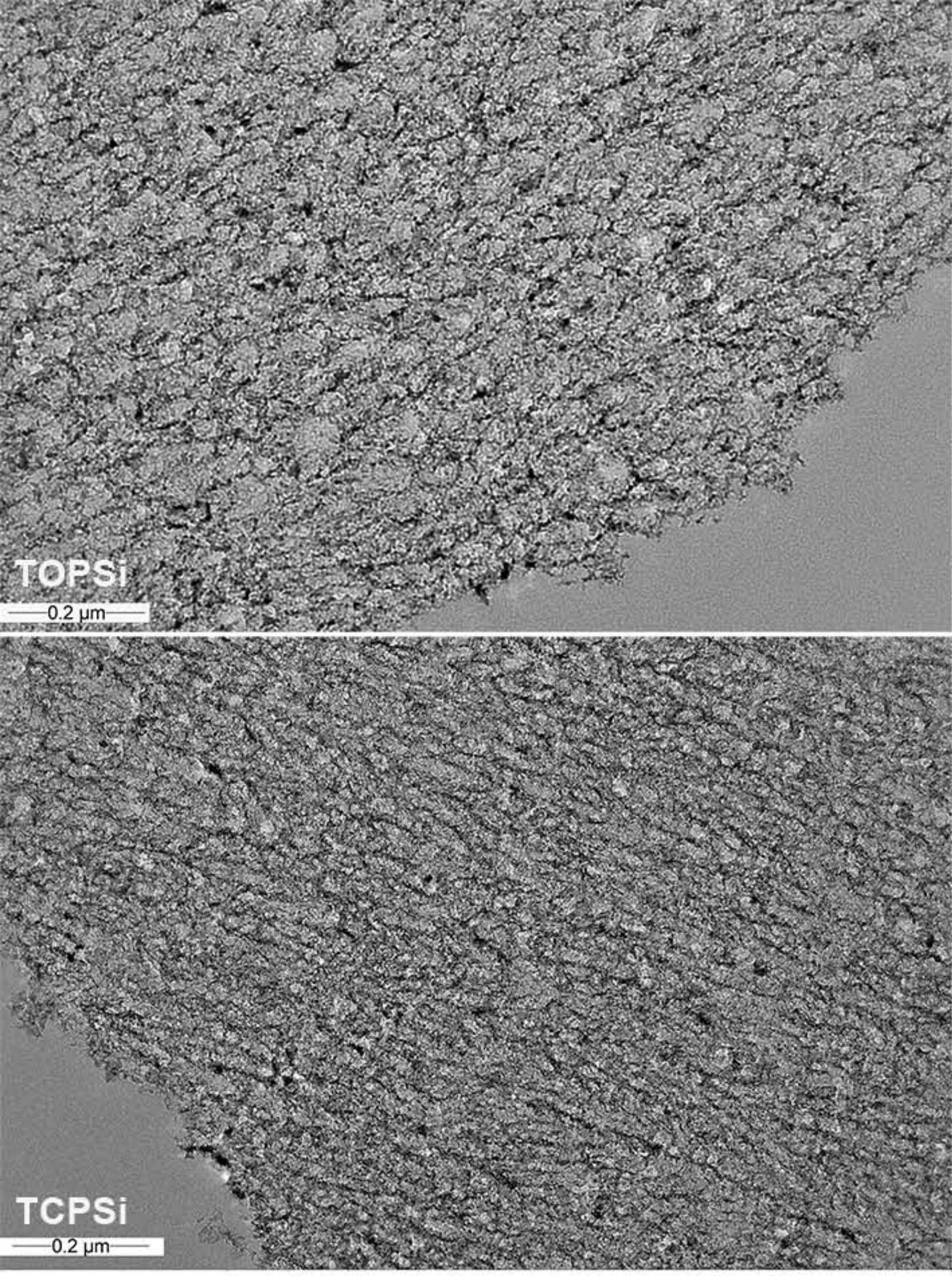
TOPSi
0.2 µm
TCPSi
0.2 µm
UnTHCPSi
0.2 µm

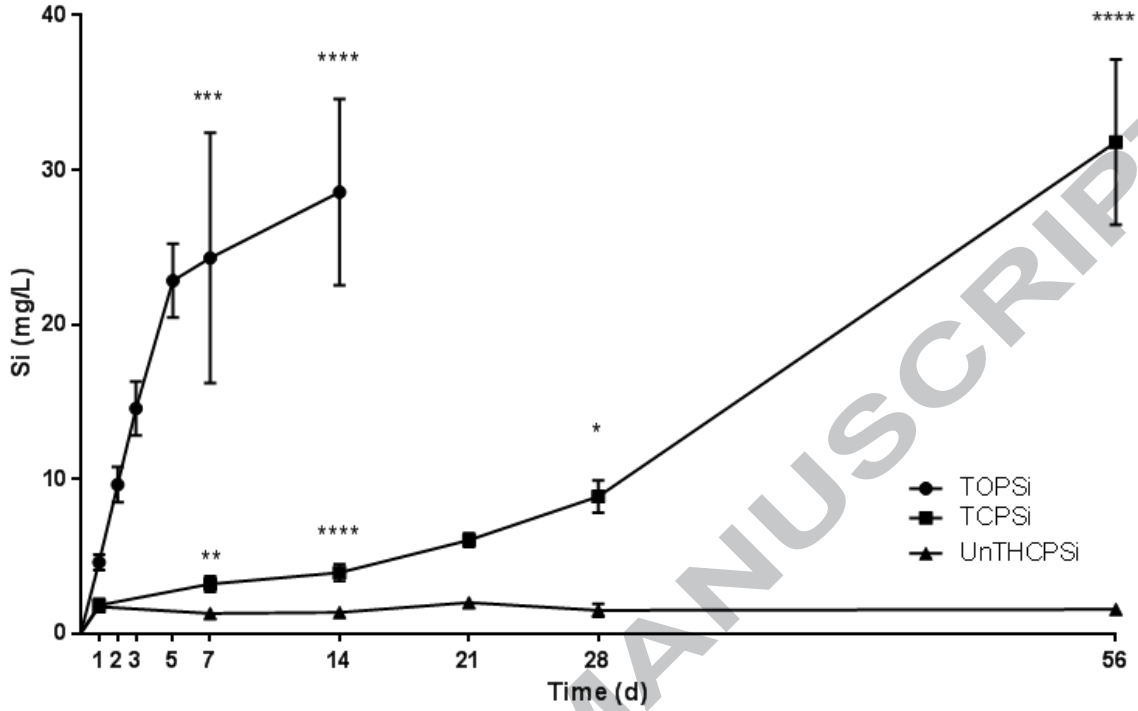

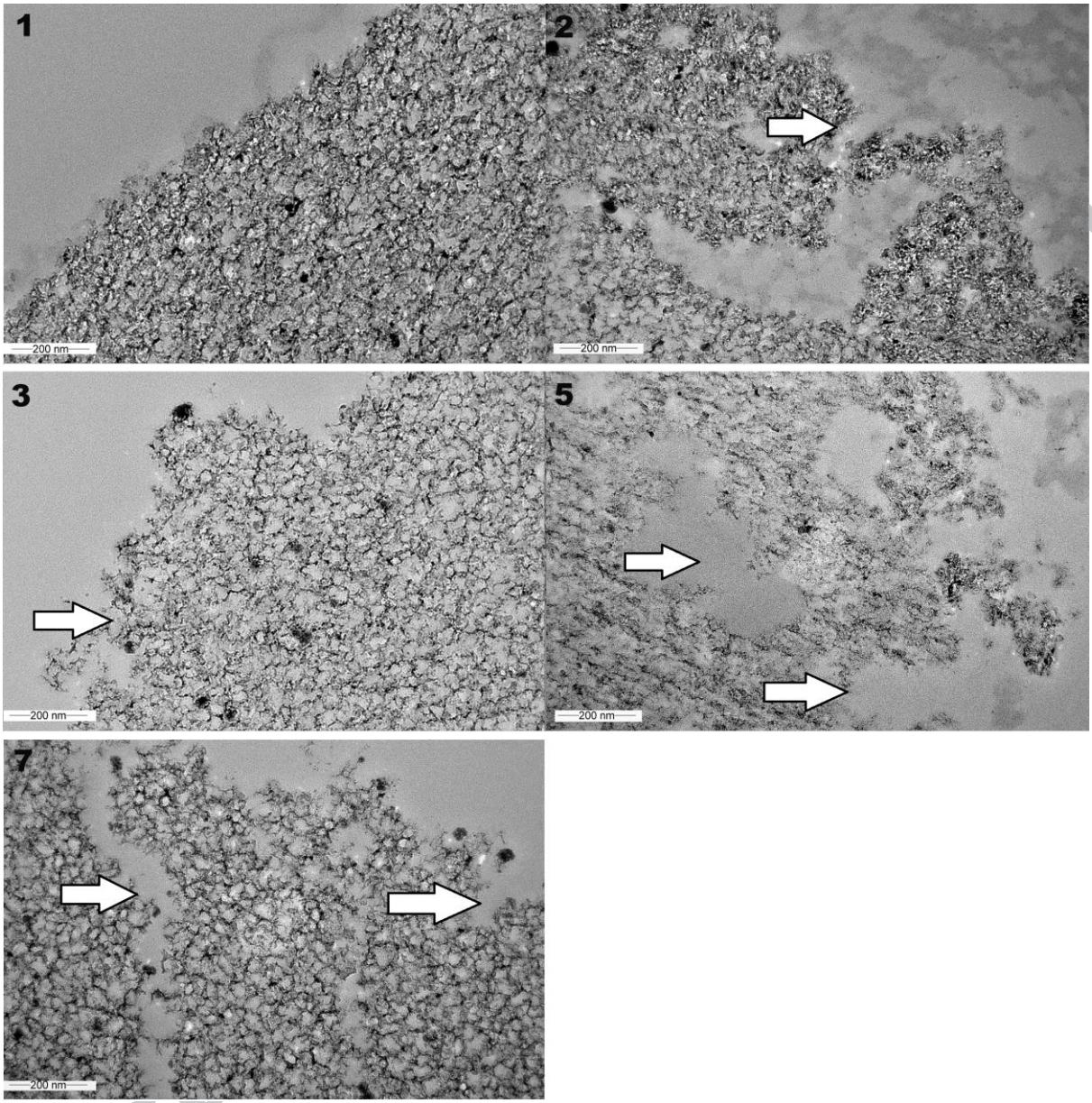
1
200 nm
2
200 nm
3
200 nm
5
200 nm
7
200 nm

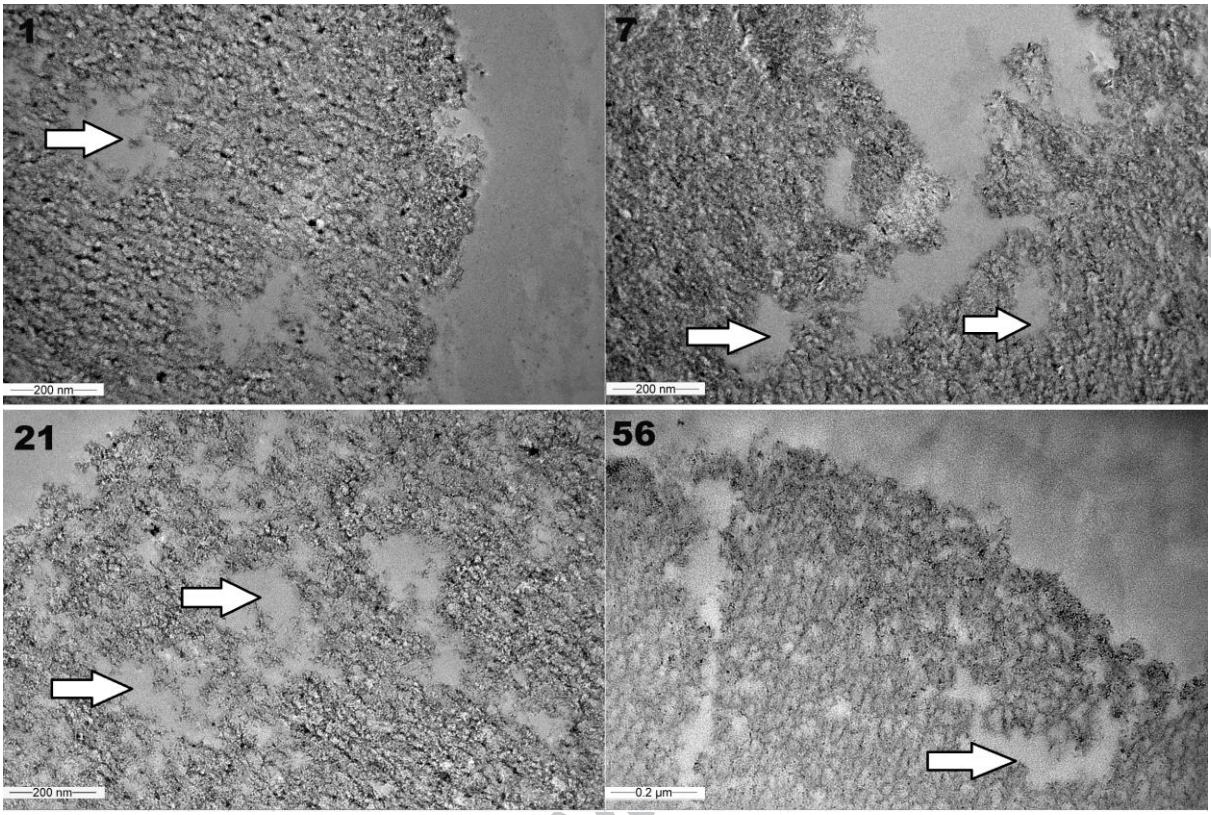

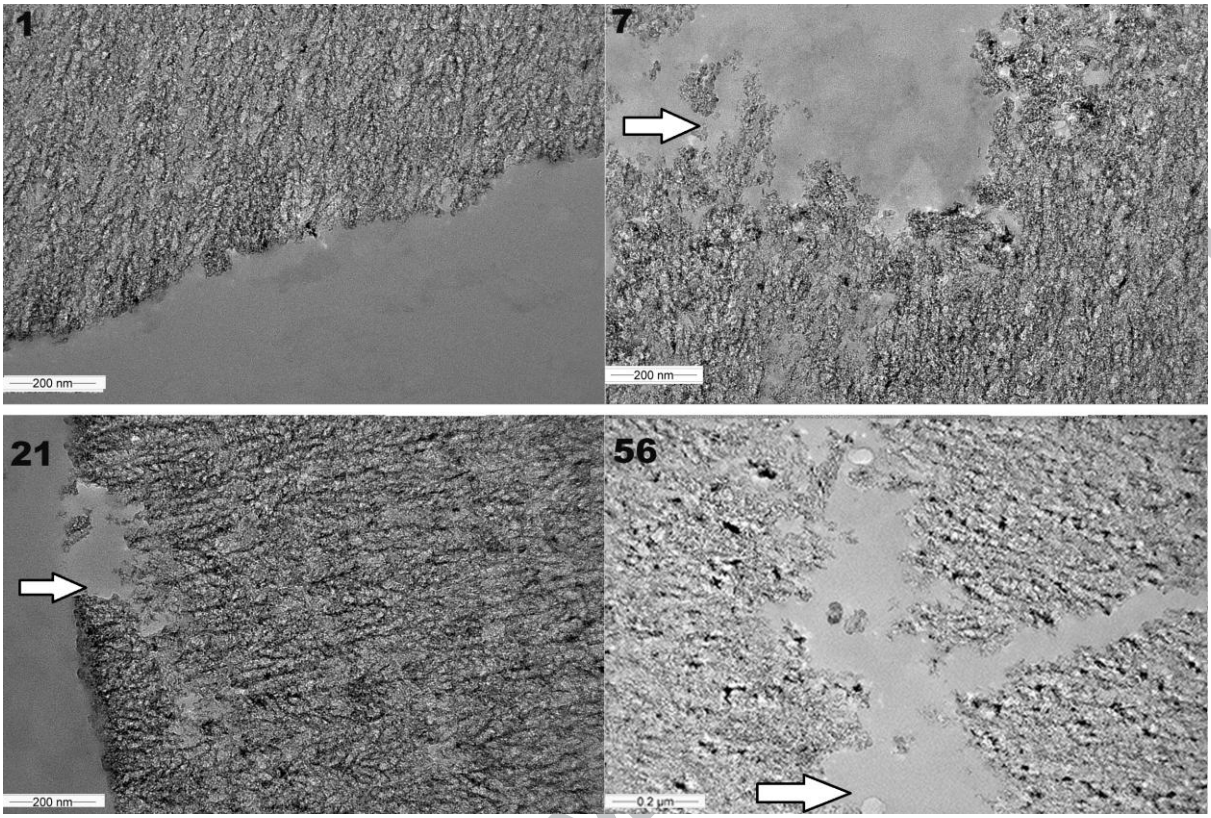

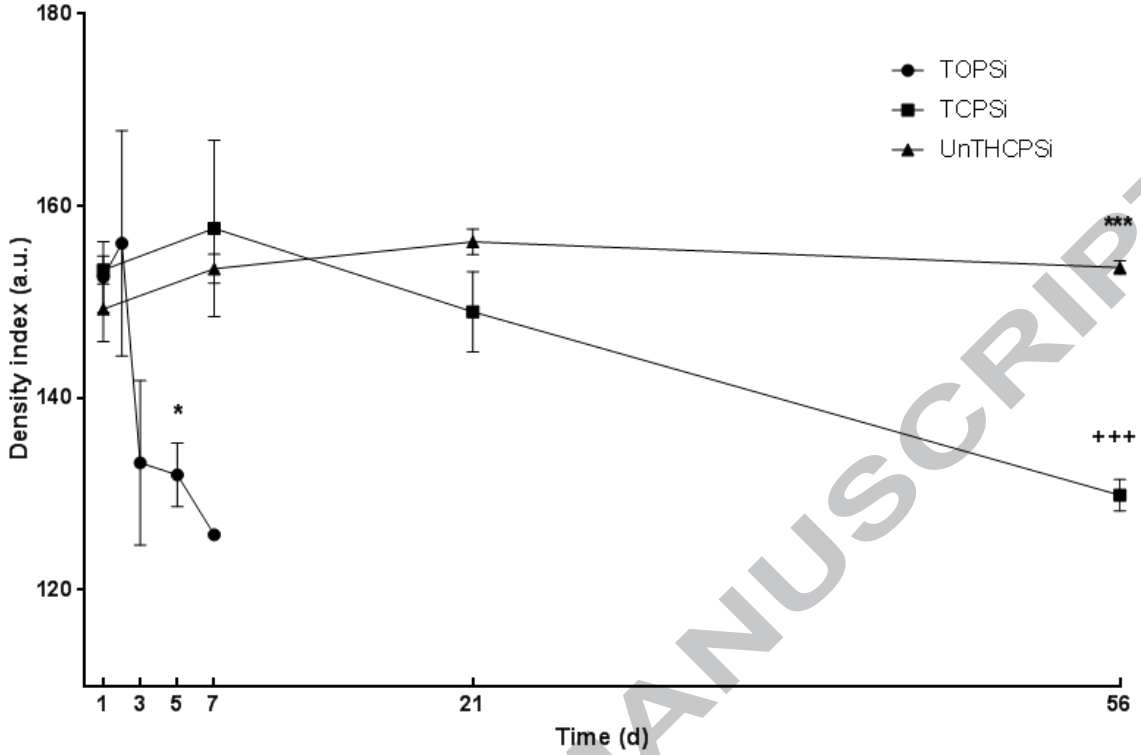

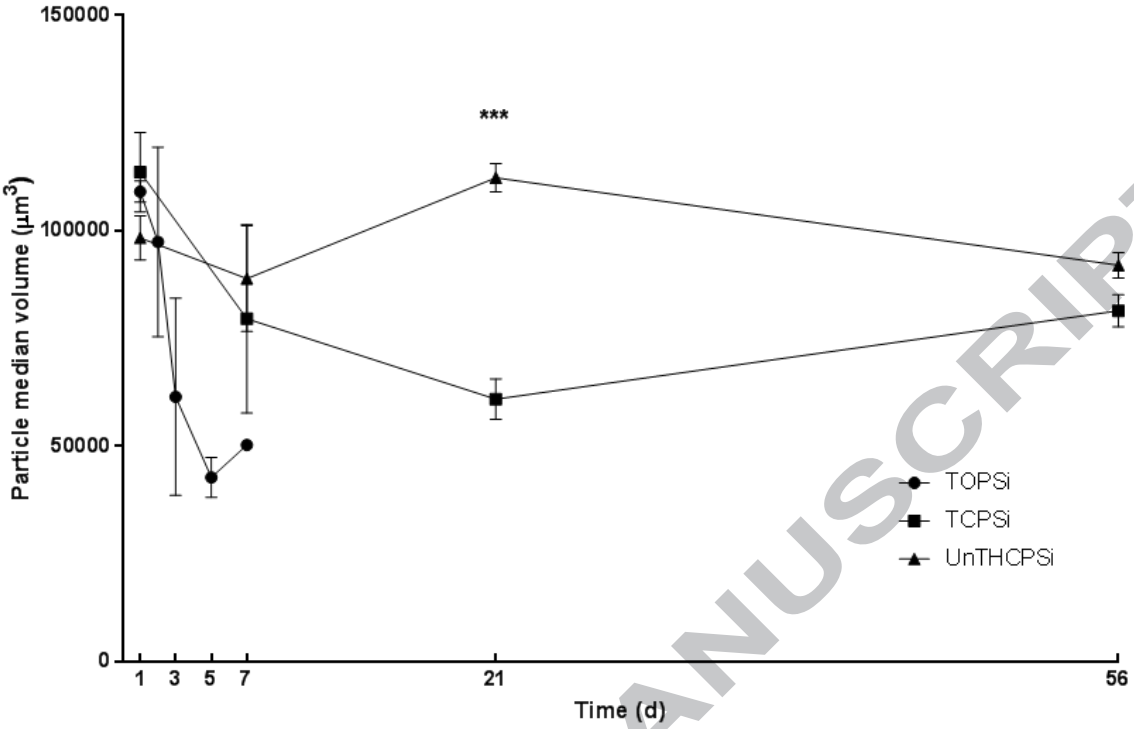

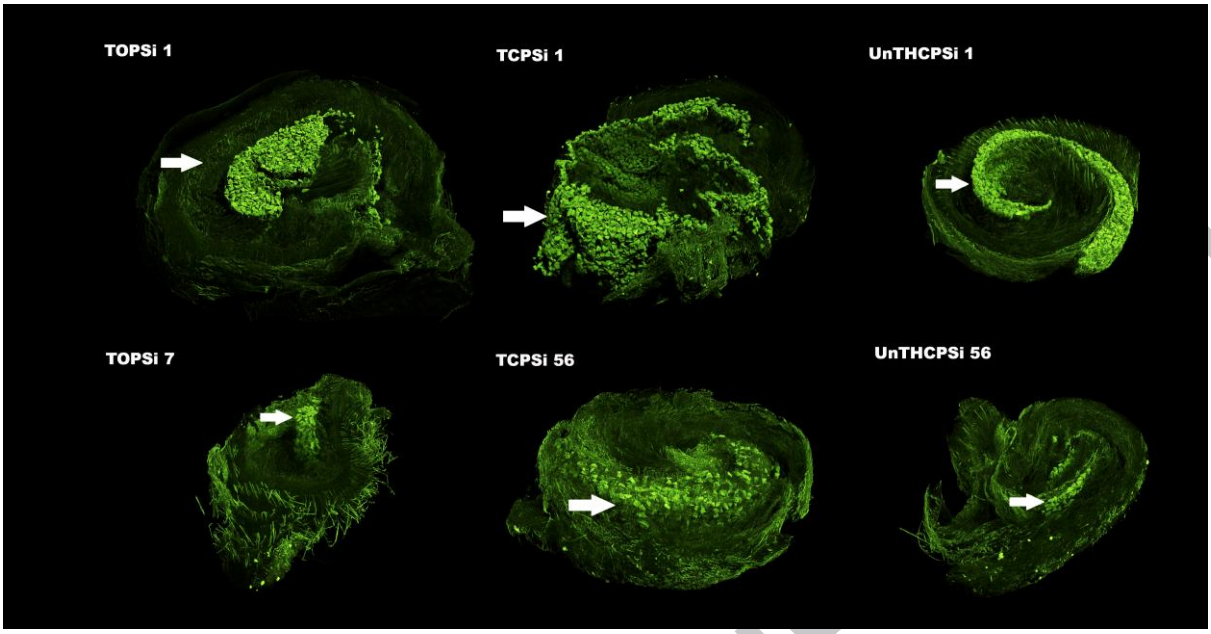

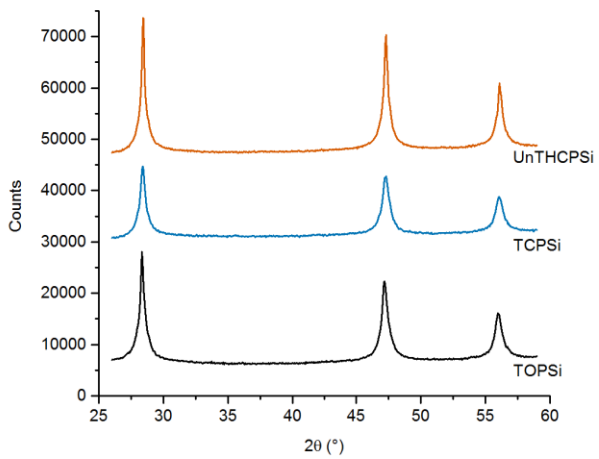

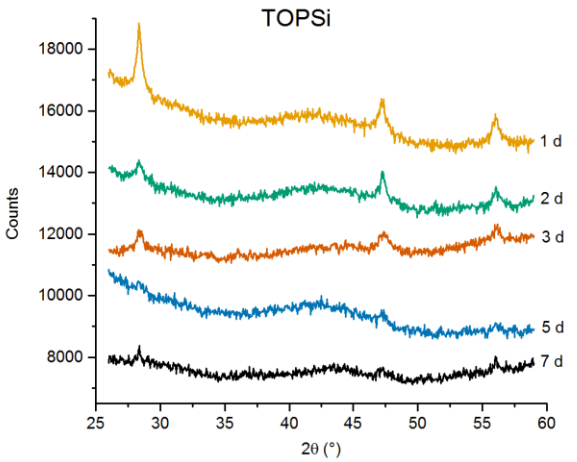

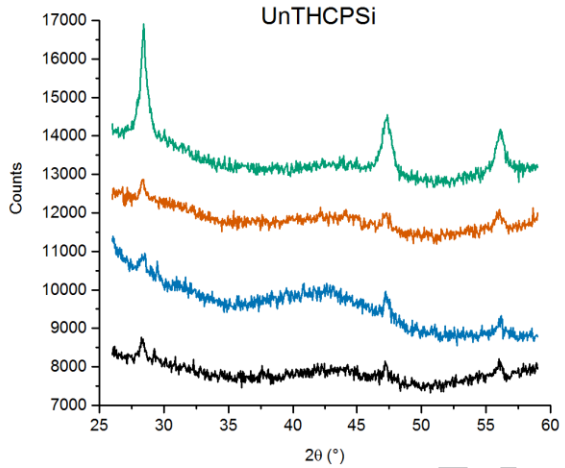

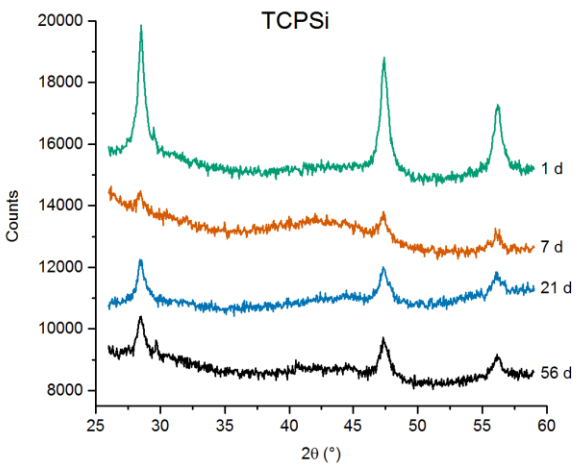

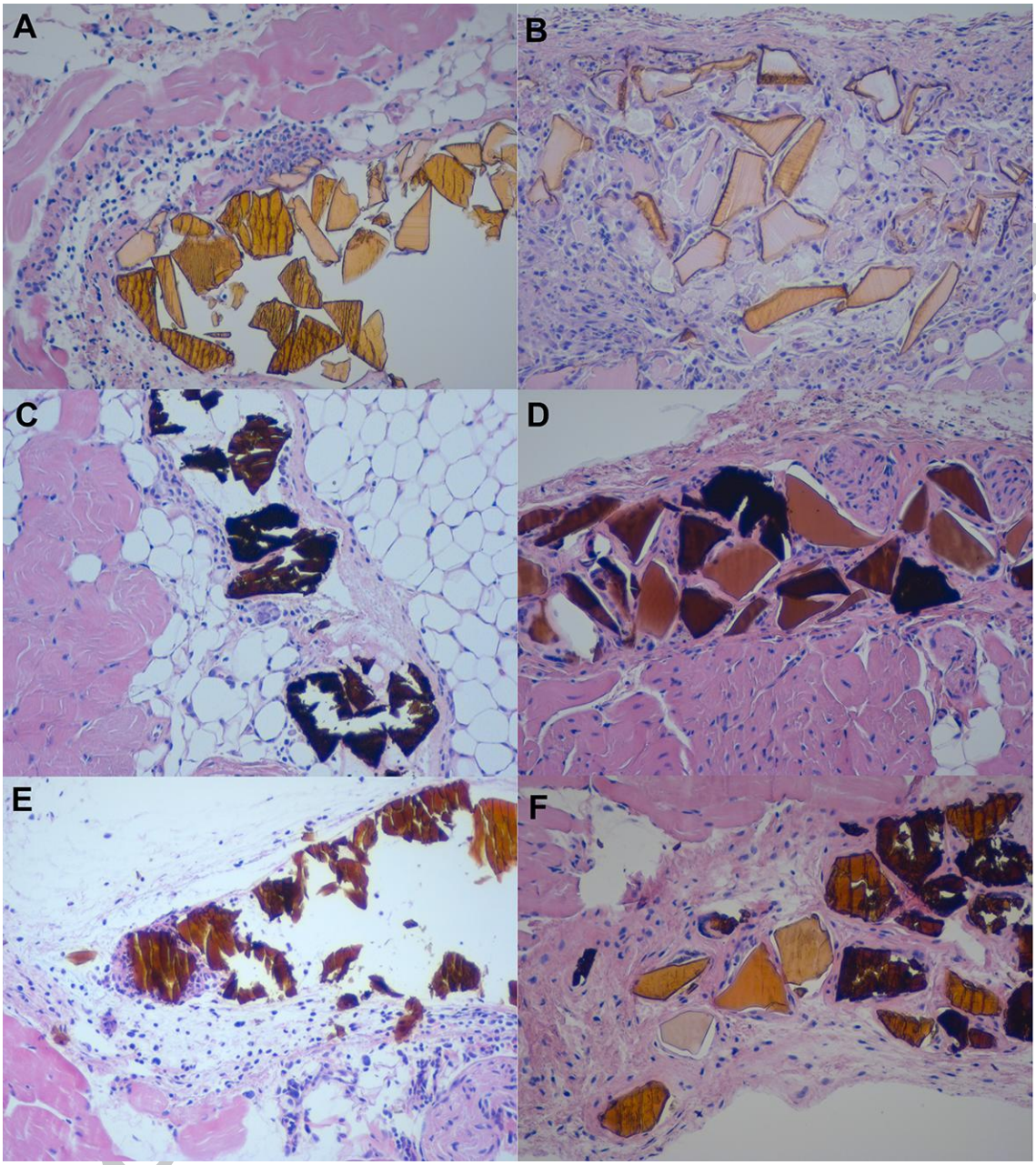

Graphical abstract